Motion Control of a Soft Circular Crawling Robot via Iterative Learning Control*

Haozhen Chi[1] Xuefang Li[2] Wenyu Liang[3] Yan Wu[3] Qinyuan Ren[1,4]

Abstract— **Soft robots have recently evoked extensive attention due to their abilities to work effectively in unstructured environments. As an actuation technology of soft robots, dielectric elastomer actuators (DEAs) exhibit many intriguing attributes such as large strain and high energy density. However, due to nonlinear electromechanical coupling, it is challenging to accurately model a DEA, and further it is difficult to control a DEA-based soft robot. This work presents a novel DEA-based soft circular crawling robot. The kinematics of the soft robot is explored and a knowledge-based model is developed to facilitate the controller design. An iterative learning control (ILC) method then is applied to control the soft robot. By employing ILC, the performance of the robot motion trajectory tracking can be improved significantly without using a perfect model. Finally, several numerical studies are conducted to illustrate the effectiveness of the ILC.**

I. INTRODUCTION

Benefit from the feature of flexible materials, soft robots undoubtedly have higher motion complexity than conventional rigid robots. Soft robots can stretch, bend and twist in a completely new way, therefore they possess great environmental adaptability, motion sensitivity and morphological diversity. In view of these, soft robots have high research value and application prospects.

This paper presents a novel soft circular crawling robot capable of omni-directional motion and explores the motion control issue of such robot. The body of the soft robot belongs to a class of dielectric elastomer actuators (DEAs) which have many similar properties of biological muscles such as fast response, large strain and high energy density. Moreover, four electro-adhesion actuators are adopted as the robot feet to provide adaptive and low-power consumption adhesion action. The use of the DEA and the electro-adhesion actuators render the robot to be light weight and fast in response. Furthermore, inspired by the natural inchworm, the robot can obtain stable locomotion through alternate expansion/contraction of the body and adhesion/detachment of the feet.

As one of the key steps in designing a controllable DEA based soft robot, it is necessary to find out how to control the DEA accurately. In [1], a feed-forward control approach is proposed for a planar DEA. However, due to the lack of feedback information, this control scheme cannot adjust the control output to pursue a better performance, which limits its application. To enhance the robustness of the control system, feedback control schemes are considered in several studies, the notable examples include the classic proportional-integral-derivative (PID) control scheme presented in [2] and the cerebellum-inspired adaptive controller proposed in [3]. It should be pointed out that these previous studies on the control of DEAs are mostly restricted at isolated actuators with simple geometries. So far, although various soft robots driven by DEAs have been developed [4]–[6], few studies have focused on the motion control of the DEA based soft robots, which greatly hindered these soft robots from practical applications.

Based on the proposed soft robot, this work aims to address the motion control problem of the robot via iterative learning control (ILC), which is essential for both motion control and motion planning [7]. The motivation of adopting ILC for the soft robot control comes from three aspects. Firstly, a regular desired sequence motion trajectory is critical to drive the robot in a cluttered environment [8]. Given by this, it needs to study the working principle of DEA at first, which can be found that each of the action cycle is only open-loop and uncontrollable. In this way, the specific action of a single cycle of DEA can be only adjusted by the input signals. Therefore, in order to improve the robot trajectory tracking performance, the input and output information of the DEA control system in the past cycles are generally used to formulate the input signal for the next iteration and ILC is usually designed to handle such repetitive tasks. Secondly, as pointed out in [9], [10], one of the main challenges of the DEA based soft robot control is that it is difficult to obtain an accurate model. As far as we know, ILC is a partial model-free control method. In other words, a great control performance can still be achieved even without the specific system parameters. Thirdly, it has been proved that the design and implementation of ILC is not so difficult which has a general promotion significance, and the application process will not be very high complexity. At present, such controllers have been widely applied in many fields of practice, such as the motion control with mobile robots, manipulators, electric motors and fish robots, etc. This paper will demonstrate the effectiveness of ILC in the motion control of soft robots and establish the foundation for future work.

The rest of this paper is organized as follows. Section II details the robot prototype. The dynamical model of the

*This research is partially supported by the Agency for Science, Technology and Research (A*STAR) under its AME Programmatic Funding Scheme (Project #A18A2b0046), and partially supported by the Open Research Project of the State Key Laboratory of industrial Control Technology, Zhejiang University, China (No. ICT1900315).

[1]College of Control Science and Engineering, Zhejiang University, P.R. China

[2]Department of Electrical and Electronic Engineering, Imperial College London, UK.

[3]Institute for Information Research, A*STAR, Singapore.

[4]Corresponding author.

soft robot is built in Section III. Section IV explores the ILC design with its convergence analysis. Furthermore, the effectiveness of the proposed ILC scheme is verified by simulations in Section V. Finally, in Section VI, a brief conclusion is given.

II. A SOFT CIRCULAR CRAWLING ROBOT

A. Robot Prototype

The prototype of the soft crawling robot to be discussed in this paper is exhibited in Fig. 1. The robot is mainly composed of two modules: a circular DEA as the robot body and four electro-adhesion actuators (EAs) as the robot feet. During the actuation, the DEA is used to generate the whole deformation reversibly, while the EAs help the robot grasp the surface. In addition, in order to reduce the frictional resistance generated during the movement, four sets of passive omni-directional auxiliary wheels are installed. Moreover, an embedded micro-controller (Arduino UNO) is used to receive external sensor signals and calculate the specific execution steps by the internal program for the actual robot control.

Figure 2 illustrates the configuration of the DEA, which is actually a capacitor consisting of a VHB membrane sandwiched by two sheets of compliant electrodes. Upon application of high voltage, because of the incompressibility of the VHB 4910 material, the membrane will undergo an isovolumetric deformation under the action of voltage-induced Maxwell stress [11] which is mainly represented by thickness reduction and area expansion in this study. In the actual fabrication process, the membrane with a thickness of 1 mm and the radius of 25 mm is selected. Next, the membrane is subjected to a physical equal-biaxial pre-stretching to evenly expand its area by 16 times, meanwhile two Acrylic frames are used for constraining or fixing to maintain the pre-stretched state. Thus, the radius of the membrane as the pre-stretched state will reach 100 mm. Finally, compliant electrodes are scribbled on the both surfaces of the membrane for the conductivity of the electricity.

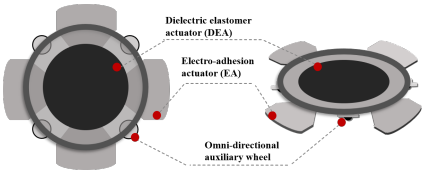

Fig. 1. Soft mobile robot prototype.

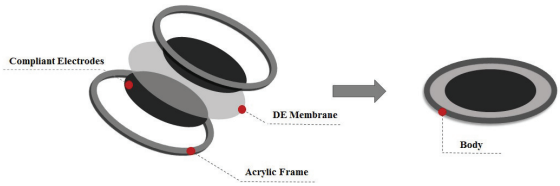

Fig. 2. Fabrication process of the robot body.

Thus, the membrane remains pre-stretched under mechanical constraints. When the voltage is applied, the membrane expands omni-directionally, and restore to the initial state with the voltage off, consequently bringing about reversible deformation process.

With the deformation ability caused by the DEA, some additional components are needed to convert the deformations into displacements. In this study, four electro-adhesion actuators illustrated in Fig. 3 are added into the robot design as the robot feet, which allow the robot move on the substrate freely.

The fabrication of this kind of actuators is given as follows. At first, the designed electrode pattern with the precise dimension shown in Fig. 3(b) should be drawn on a plain A4 paper. Thereafter, two regions enclosed by the lines would be coated with graphite using a 2B pencil to form the conductive regions. Finally, each of the separate modules was bonded together with pieces of VHB 4910 membrane (including conductive layers, Acrylic board and foot connectors). It should be noted here that the bonding material used for adhesion (such as VHB 4910 adopted herein) is required to ensure insulation to prevent the electrodes from being short-circuited via external substances.

As shown in Fig.4, when a high voltage is applied to the conductive regions of the electro-adhesion actuator, the positive and negative charges would be continuously accumulated on the conductive layer and cannot be neutralized because a complete loop is not formed. Under the effect of the accumulated charge, a high electric field is shaped between the conductive layer and the ground, thereby forming an opposite induced charges on the substrate. Thus, under the principle of electrostatic attraction, an electro-adhesive force would be generated so that the actuator can be fixed on the substrate [12]. Additionally, in order to avoid the charge neutralization, an insulating layer (e.g., paper) is needed between the conductive layer and the substrate. Furthermore, in the absence of voltage, the charges accumulated on the conductive layer will disappear, so as the induced charges and the electro-adhesion force, resulting in reversible adhesion.

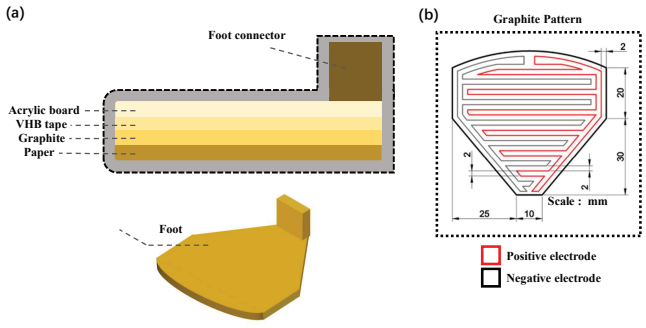

Fig. 3. Schematic of the robot foot. (a) exploded view, (b) dimensions of the electrode pattern.

B. Locomotion Mechanism

Due to the contribution of the four feet, the robot is able to realize 2D planar motion, which is represented by the linear motion in the two perpendicular directions. Because of the consistent movement mechanism in both directions, here we only take a single direction motion as an example exhibited in Fig. 5 (the other directional EAs do not effect the robot, so they are ignored in the following description, and the whole process is in a non-power supply state; while the EA in the positive of this direction is defined as the forefoot, the negative is treated as the rear foot): as the first step of the loop, the voltage applied to forefoot is removed, only the rear foot is powered for its adhesion, and the body is supplied with power as well to cause the body expanding, thereby pushing the forefoot forward; thereafter the body expands to a certain extent, the forefoot is reattached to fix on the substrate, while the voltage of the body and the rear foot is removed which means they would return to the initial state, thus the rear foot will be pulled towards the DEA's center due to the shrink of the body. Consequently, the robot achieves a cycle-by-cycle forward locomotion. Furthermore, by reversing the actuation sequence of the EAs, the robot is able to move forward and backward, respectively.

By this way, the robot is able to realize 2D omni-directional motion (forward, backward, left and right). Simultaneously, this type of movement exhibits a high degree of stability, which is particularly suitable for unstructured environments.

III. Modeling

Dynamic modeling of the robot body is essential for the controller design. The previous studies of modeling a DEA are generally based on the theory of DE [13]–[15]. However, the results of these studies are generally described by several sets of partial differential equations, and the expression of those equations greatly reduce their practicality in model-based controller design, which can not meet complex control objectives. In this section, a knowledge-based data-driven method is employed to model the DEA of the soft robot.

Due to the similarity between biological muscles and DE materials in terms of viscoelasticity, a simplified spring-dashpot model is employed to describe the physical analog [16]. According to the locomotion of the soft robot, the robot body is treated as a single elastic element along the motion direction while the overall body shape change is ignored. As shown in Fig.6, the voltage induced force F_{active} can be considered as the product of an equivalent Maxwell stress with an equivalent cross-sectional area of the body, which is related to the length change. Since Maxwell stress is proportional to the electric field, F_{active} can be written as

$$F_{active} = V^2(\alpha x + \beta), \tag{1}$$

where V is the voltage applied in kV and x represents the length change related to deformation. According to [9], $\alpha x + \beta$ describes the mapping between the voltage induced force with different length changes and different voltages. α and β can be determined using the least square fitting method.

As pointed in [15], the static stretch force is described by a linear spring with stiffness k. The spring-dashpot parameters include the spring deformation x_h, the spring stiffness k_h and the viscous friction coefficient c_h $(h = 1, 2, ..., N)$. The model uncertainties mainly come from the equivalent mass $\tilde{m}$ of the system and the resistance force ζ during the motion. The dynamic equations are given as

$$\tilde{m}\ddot{x} = -kx - \sum_{h=1}^{N} k_h x_h + F_{active} - \zeta sign(\dot{x}), \tag{2}$$

$$k_h x_h = c_h(\dot{x} - \dot{x_h}), h = 1, 2, \cdots, N. \tag{3}$$

In this work, the number of spring-dashpot pairs is selected as $N = 3$, which can finally well predict the dynamics of the DEA. The model developed in this work is completely a simplified version compared to its actual model, but will be more suitable for the complex geometries DEAs that are difficult to describe analytically. Thus, converting the above differential equations into the state-space model, we can have

$$\dot{X} = AX + Bu, \tag{4}$$

$$y = CX. \tag{5}$$

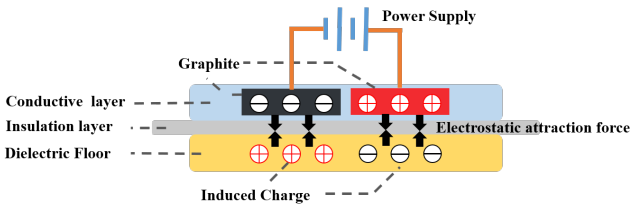

Fig. 4. Working principle of the EA.

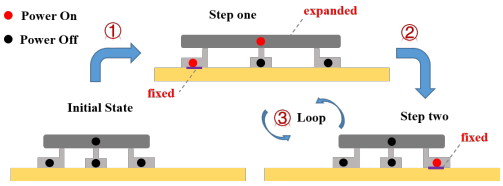

Fig. 5. Robot locomotion.

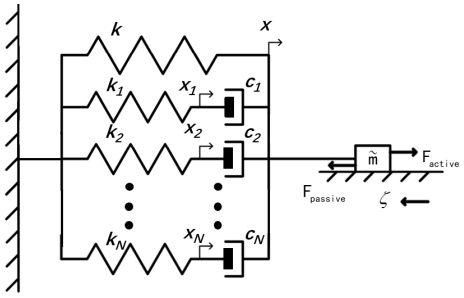

Fig. 6. Dynamic model of the DEA

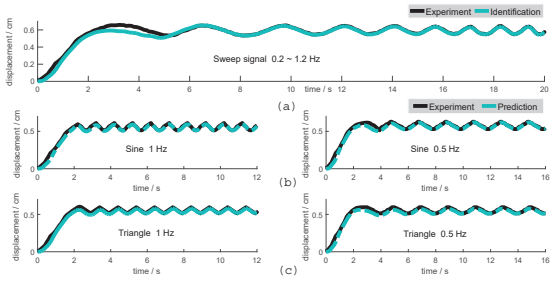

Fig. 7. Experimental results of model identification and validation. (a) identification result applying a sweep voltage signal, (b) and (c) validation results applying sine voltage signals and triangle voltage signals, respectively.

where

$$u = \frac{F_{active} + \tilde{f}}{\tilde{m}}, F_{active} \geq 0, \tag{6}$$

$$\tilde{f} = -\zeta sign(\dot{x}), \tag{7}$$

$$X = \begin{bmatrix} x_1 & x_2 & x_3 & x & \dot{x} \end{bmatrix}^T, \tag{8}$$

$$A = \begin{bmatrix} -k_1/c_1 & 0 & 0 & 0 & 1 \\ 0 & -k_2/c_2 & 0 & 0 & 1 \\ 0 & 0 & -k_3/c3 & 0 & 1 \\ 0 & 0 & 0 & 0 & 1 \\ -k_1/\tilde{m} & -k_2/\tilde{m} & -k_3/\tilde{m} & -k/\tilde{m} & 0 \end{bmatrix}, \tag{9}$$

$$B = \begin{bmatrix} 0 & 0 & 0 & 0 & 1 \end{bmatrix}^T, \tag{10}$$

$$C = \begin{bmatrix} 0 & 0 & 0 & 1 & 0 \end{bmatrix}. \tag{11}$$

The spring-dashpot coefficients k_h and c_h are determined from the dynamic responses of the actuator by experimentally identification. First of all, the DEA is driven by a sinusoidal voltage signal with the frequency of 1 Hz, amplitude of 0.36 kV and offset of 3 kV, and then the MATLAB System Identification Toolbox is used to estimate these parameters according to the above equations and the experimental data. As shown in Fig. 7, besides the identification, several basic signals (sine wave and triangle wave) of different frequencies are also employed to verify the identified model. Finally, we get the proper parameters shown in Table I. In addition, the equivalent mass $\tilde{m}$ is 0.12 kg and the resistance force ζ is measured to be $0.1\tilde{m}g$, where g presents the gravity acceleration. As a result, this model matches the experimental data and well predicts the creep under different voltage signals.

TABLE I
THE IDENTIFIED MODEL PARAMETERS

$\tilde{m}$ (kg)	0.12	k_1 (N · cm^{-1})	34.64
ζ (N)	$0.1\tilde{m}g$	k_2 (N · cm^{-1})	15.2
k (N · cm^{-1})	3.456	k_3 (N · cm^{-1})	0.0396
α (N · cm^{-1}1 · kV^{-2})	3.6	c_1 (N · cm · s^{-1})	0.4
β (N · kV^{-2})	-0.25	c_2 (N · cm · s^{-1})	5.067
		c_3 (N · cm · s^{-1})	12

IV. CONTROLLER DESIGN

In this work, the control objective is to drive the robot to follow a predefined target trajectory, which will be realized by using ILC. First of all, the system dynamics of the robot in iteration domain is

$$X_k = AX_k + Bu_k, \tag{12a}$$
$$y_k = CX_k, \tag{12b}$$

where k is the iteration index and

$$u_k \triangleq \frac{V_k^2(\alpha x_k + \beta) - \zeta \text{sign}(\dot{x}_k)}{\tilde{m}} \tag{13}$$

is a virtual control input to the system (the actual control input to the robot is the voltage V_k).

To facilitate the convergence analysis, it is assumed that the target trajectory y_d is generated by the following dynamical system

$$X_d = AX_d + Bu_d, \tag{14a}$$
$$y_d = CX_d. \tag{14b}$$

This is a common assumption in the ILC field. The control objective is to find a sequence of u_k such that the system output y_k can track the desired target y_d as closely as possible.

It is clear from the modeling section that $CB = 0$, i.e., the relative degree of the system is higher than 1, which motivates us to design a higher-order ILC scheme. By paying attention to the property $CAB = 1$, a D^2 type of ILC law is proposed

$$V_k = \sqrt{\frac{u_k\tilde{m} + \zeta \text{sign}(\dot{x}_k)}{\alpha x_k + \beta}}, \tag{15a}$$
$$u_{k+1} = u_k + \gamma \ddot{e}_k. \tag{15b}$$

where γ means the learning gain that determines the overall speed of the iterative process.

The convergence analysis of the proposed controller is given below.

Denote $e_k \triangleq y_d - y_k$, $\Delta X_k \triangleq X_d - X_k$, $\Delta u_k \triangleq u_d - u_k$. By considering the ILC law (15b) and the definition of Δu_k, it gives

$$\begin{aligned} \Delta u_{k+1} &= u_d - u_{k+1} \\ &= u_d - (u_k + \gamma \ddot{e}_k) \\ &= \Delta u_k - \gamma \ddot{e}_k. \end{aligned} \tag{16}$$

Since $\Delta \dot{X}_k = A\Delta X_k + B\Delta u_k$ and $CB = 0$, we can obtain

$$\begin{aligned} \dot{e}_k &= \dot{y}_d - \dot{y}_k \\ &= C\Delta \dot{X}_k \\ &= C(A\Delta X_k + B\Delta u_k) \\ &= CA\Delta X_k \end{aligned} \tag{17}$$

which therefore implies that

$$\begin{aligned}\ddot{e}_k &= CA\Delta\dot{X}_k \\ &= CA^2\Delta X_k + CAB\Delta u_k. \end{aligned} \tag{18}$$

By substituting (18) into (16), since $CAB = 1$, it has

$$\begin{aligned}\Delta u_{k+1} &= (1-\gamma CAB)\Delta u_k - \gamma CA^2\Delta X_k \\ &= (1-\gamma)\Delta u_k - \gamma CA^2\Delta X_k. \end{aligned} \tag{19}$$

As the solution of (12a) is

$$X_k(t) = e^{At}X_k(0) + \int_0^t e^{A(t-\tau)}Bu_k(\tau)d\tau, \tag{20}$$

then we have

$$\Delta X_k(t) = \int_0^t e^{A(t-\tau)}B\Delta u_k(\tau)d\tau, \tag{21}$$

provided that $X_d(0) = X_k(0)$.

By taking norm on both sides of (21), it yields

$$\|\Delta X_k(t)\| = \int_0^t e^{a(t-\tau)}b\|\Delta u_k(\tau)\|d\tau, \tag{22}$$

where $a \geq \|A\|$ and $b \geq \|B\|$. Define $\|g(t)\|_\lambda \triangleq \sup_{t\in[0,T]} e^{-\lambda t}\|g(t)\|$, then (22) gives

$$\begin{aligned}\|\Delta X_k(t)\| &\leq be^{at}\int_0^t e^{(\lambda-a)\tau}d\tau\|\Delta u_k(t)\|_\lambda \\ &= b\frac{e^{\lambda t}-e^{at}}{\lambda-a}\|\Delta u_k(t)\|_\lambda. \end{aligned} \tag{23}$$

Hence we have

$$\begin{aligned}\|\Delta X_k(t)\|_\lambda &= \sup_{t\in[0,T]} e^{-\lambda t}\|\Delta X_k(t)\| \\ &\leq b\sup_{t\in[0,T]}\frac{1-e^{-(\lambda-a)t}}{\lambda-a}\|\Delta u_k(t)\|_\lambda \\ &\leq b\frac{1-e^{-(\lambda-a)T}}{\lambda-a}\|\Delta u_k(t)\|_\lambda \\ &\triangleq O(\lambda^{-1})\|\Delta u_k(t)\|_\lambda \end{aligned} \tag{24}$$

for a sufficiently large $\lambda > a$.

By taking the λ-norm on both sides of (19) and applying (24), it has

$$\|\Delta u_{k+1}\|_\lambda = (|1-\gamma| + \gamma\|CA^2\|O(\lambda^{-1}))\|\Delta u_k\|_\lambda. \tag{25}$$

If γ is designed properly such that $|1-\gamma| < 1$ (i.e., $0 < \gamma < 2$), there exists $\delta > 0$ such that $|1-\gamma| + \delta < 1$.

By selecting a sufficiently large λ, the following inequality can be satisfied

$$\gamma\|CA^2\|O(\lambda^{-1}) < \delta.$$

Therefore, the convergence of $\|\Delta u_k\|_\lambda$, i.e., Δu_k, has been proven. According to the convergence of Δu_k and the inequality (24), it is obvious that

$$\lim_{k\to\infty}\Delta X_k = 0. \tag{26}$$

Furthermore, because $e_k(t) = C\Delta X_k(t)$, the convergence of $e_k(t)$, $t \in [0,T]$, can be obtained immediately.

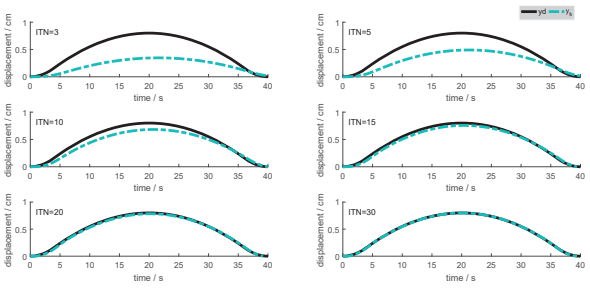

Fig. 8. The simulation results of motion trajectory profiles with Arch-type signal under different iterations. ITN indicates the current iteration number.

V. Simulation

In order to verify the effectiveness of the proposed ILC scheme, some simulations are conducted in this section.

The model parameters used in the simulation are detailed in Table I. In order to verify the effectiveness of the motion trajectory tracking performance with the ILC controller, it is necessary to develop a desired trajectory for testing. In this section, two representative and realistic trajectories are used.

Firstly, because the target in the tracking is the motion trajectory, there is bound to be a common process of shuttle in the actual application. Therefore, by simplifying this process, an arch-type trajectory is constituted as shown in (27).

$$y_{d,Arch}(t) = \begin{cases} \dfrac{t^2}{100} & (0 \leq t \leq 4) \\ -\dfrac{(t-20)^2}{400} + 0.8 & (4 < t \leq 36) \\ \dfrac{(t-40)^2}{100} & (36 < t \leq 40) \\ 0 & (t > 40) \end{cases}, \tag{27}$$

According to the design process of ILC controller in Section IV, only the learning gain γ and the initial input signal u_0 need to be adjusted for a better performance. In this simulation, set $u_0 = 0$ and $\gamma = 0.05$ based on multiple considerations. As can be seen from Fig. 8, the simulated trajectory can perfectly track the desired trajectory. In other words, the soft robot can be actuated according to a certain desired trajectory under the control of ILC, which will greatly improve its manipulability. For more details, the deviation between the motion trajectory and the desired trajectory is relatively large in the case of the early iterations, but would gradually decrease as the number of iterations increases and eventually approach near zero after 30 times of iteration. This result also proves the effectiveness of the ILC controller, indicating that the control effect would be significantly improved as the iteration increases.

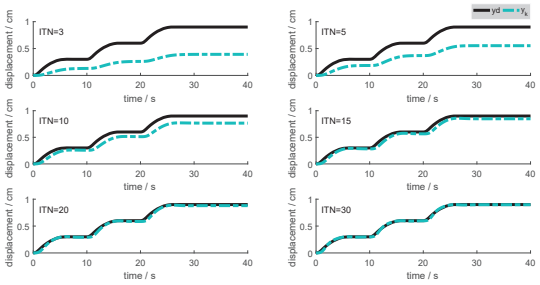

Fig. 9. The simulation results of motion trajectory profiles with Ladder-type signal under different iterations. ITN indicates the current iteration number.

$$y_{d,Ladder}(t)=\begin{cases}\dfrac{t^2}{20} & (0\le t\le 1)\\ -\dfrac{(t-6)^2}{100}+0.3 & (1<t\le 6)\\ 0.3 & (6<t\le 10)\\ \dfrac{(t-10)^2}{20}+0.3 & (10\le t\le 11)\\ -\dfrac{(t-16)^2}{100}+0.6 & (11<t\le 16)\\ 0.6 & (16<t\le 20)\\ \dfrac{(t-20)^2}{20}+0.6 & (20\le t\le 21)\\ -\dfrac{(t-26)^2}{100}+0.9 & (21<t\le 26)\\ 0.9 & (t>26)\end{cases}, \quad (28)$$

Secondly, inspired by the idea of phased movement process, another trajectory is designed. In general, for the purpose of stability, intermittent motion restrictions would be imposed during the design. For example, when a robot is required to move from point A to point B, there will generally be an intermediate transition point for a short stay to prevent the deviation between two adjacent displacement from being too large, otherwise it is prone to breakdown. Therefore, based on this consideration, a ladder-type trajectory is formed as (28).

Similarly, set the initial signal $u_0 = 0$ and the learning gain $\gamma = 0.05$ to keep the simulation conditions consistent. As shown in Fig. 9, the final results are also similar to the previous one. In other words, the tracking performance is also great for this trajectory by applying the ILC scheme.

According to the simulation results shown above, it can be concluded that the proposed ILC scheme is able to solve the trajectory tracking problem of the developed soft robot effectively.

VI. Conclusion

This paper demonstrates the motion trajectory tracking control of a novel DEA-based soft circular crawling robot. By virtue of the knowledge on the DEA, a simplified dynamic model is obtained by data-driven method. Although the model is a simplified version compared to its actual model, the viscoelasticity, inertia and friction is also considered and the model has the ability to predict the dynamic response of the DEA well. Therefore, this knowledge-based data-driven model is suitable for the motion controller design. Based on the dynamic model, an ILC scheme is designed and its convergence is analyzed in detail. Finally, several simulations are conducted to verify the effectiveness of the designed controller. The results show that the ILC scheme can significantly improve the motion trajectory tracking performance of the DEA-based soft robot. Motivated by its effectiveness verified in the simulation, we will study the applicability of the proposed ILC in application of the soft robot in the next research phase.

References

[1] G. Y. Gu, U. Gupta, J. Zhu, L. M. Zhu, and X. Y. Zhu, "Feedforward deformation control of a dielectric elastomer actuator based on a nonlinear dynamic model," *Applied Physics Letters*, vol. 107, no. 4, p. 836, 2015.

[2] S. Q. Xie, P. F. Ramson, D. D. Graaf, E. P. Calius, and I. A. Anderson, "An adaptive control system for dielectric elastomers," in *IEEE International Conference on Industrial Technology*, 2006.

[3] E. D. Wilson, T. Assaf, M. J. Pearson, J. M. Rossiter, S. R. Anderson, J. Porrill, and P. Dean, "Cerebellar-inspired algorithm for adaptive control of nonlinear dielectric elastomer-based artificial muscle," *Journal of the Royal Society Interface*, vol. 13, no. 122, p. 20160547, 2016.

[4] B. Paul and P. Qibing, "Advances in dielectric elastomers for actuators and artificial muscles," *Macromolecular Rapid Communications*, vol. 31, no. 1, pp. 10–36, 2010.

[5] C. Jordi, S. Michel, and E. Fink, "Fish-like propulsion of an airship with planar membrane dielectric elastomer actuators," *Bioinspiration & Biomimetics*, vol. 5, no. 2, p. 026007, 2010.

[6] W. B. Li, W. M. Zhang, H. X. Zou, Z. Peng, and G. Meng, "A fast rolling soft robot driven by dielectric elastomer," *IEEE/ASME Transactions on Mechatronics*, vol. 23, no. 4, pp. 1630–1640, 2018.

[7] D. A. Bristow, M. Tharayil, and A. G. Alleyne, "A survey of iterative learning," *IEEE Control Systems*, vol. 26, no. 3, pp. 0–114, 2006.

[8] L. Qin, Y. Tang, U. Gupta, and J. Zhu, "A soft robot capable of 2d mobility and self-sensing for obstacle detection and avoidance," *Smart Materials and Structures*, vol. 27, no. 4, 2018.

[9] J. Cao, W. Liang, Q. Ren, U. Gupta, F. Chen, and J. Zhu, "Modelling and control of a novel soft crawling robot based on a dielectric elastomer actuator," in *2018 IEEE International Conference on Robotics and Automation (ICRA)*, 2018, pp. 1–9.

[10] J. Cao, W. Liang, J. Zhu, and Q. Ren, "Control of a muscle-like soft actuator via a bioinspired approach," *Bioinspiration & Biomimetics*, vol. 13, no. 6, p. 066005, 2018.

[11] Z. Xuanhe and S. Zhigang, "Theory of dielectric elastomers capable of giant deformation of actuation," *Physical Review Letters*, vol. 104, no. 17, p. 178302, 2010.

[12] J. Guo, K. Elgeneidy, C. Xiang, N. Lohse, L. Justham, and J. Rossiter, "Soft pneumatic grippers embedded with stretchable electroadhesion," *Smart Material Structures*, vol. 27, 2018.

[13] T. Li, C. Keplinger, R. Baumgartner, S. Bauer, Y. Wei, and Z. Suo, "Giant voltage-induced deformation in dielectric elastomers near the verge of snap-through instability," *Journal of the Mechanics & Physics of Solids*, vol. 61, no. 2, pp. 611–628, 2013.

[14] S. J. A. Koh, T. Li, J. Zhou, X. Zhao, and Z. Suo, "Mechanisms of large actuation strain in dielectric elastomers," *Journal of Polymer Science Part B Polymer Physics*, vol. 49, no. 7, pp. 504–515, 2015.

[15] G. Y. Gu, U. Gupta, J. Zhu, L. M. Zhu, and X. Zhu, "Modeling of viscoelastic electromechanical behavior in a soft dielectric elastomer actuator," *IEEE Transactions on Robotics*, vol. PP, no. 99, pp. 1–8, 2017.

[16] M. Benslimane, P. Gravesen, and P. Sommer-Larsen, "Mechanical properties of dielectric elastomer actuators with smart metallic compliant electrodes," *Proceedings of SPIE - The International Society for Optical Engineering*, vol. 4695, pp. 150–157, 2002.